TOPICAL REVIEW

Coarse grain models and the computer simulation of soft materials

Steve O Nielsen, Carlos F Lopez, Goundla Srinivas and Michael L Klein[1]

Center for Molecular Modeling and Department of Chemistry, University of Pennsylvania, Philadelphia, PA 19104-6323, USA

E-mail: klein@cmm.upenn.edu

Abstract

This article presents a topical review of coarse grain simulation techniques. First, we motivate these techniques with illustrative examples from biology and materials science. Next, approaches in the literature for increasing the efficiency of atomistic simulations are mentioned. Considerations related to a specific coarse grain modelling approach are discussed at length, and the consequences arising from the loss of detail are given. Finally, a large number of results are presented to give the reader a feeling for the types of problem which can be addressed.

(Some figures in this article are in colour only in the electronic version)

Contents

[1] Author to whom reprint requests should be addressed. www.cmm.upenn.edu

1. Introduction

Experimental work on complex condensed matter spans a broad range of temporal and spatial scales, from femtosecond dynamics and atomistic detail to real-time macroscopic phenomena. Simulation methods in which each atom is explicitly represented are well established but have difficulty addressing many cooperative effects of experimental and theoretical interest. There is simply too large a gap between the timescale and spatial scale that govern typical intramolecular events and those which are relevant for collective motions. One example is the mechanical unfolding of muscle proteins where the timescale gap between simulation and experiment is about six orders of magnitude [1]. Available simulation techniques for specific timescales and spatial scales are illustrated schematically in figure 1. These techniques take a variety of approaches to reduce the level of detail in the representation of the system under study as the timescale and/or length scale grows. Bridging these disparate scales is possible with multiscale modelling [2–5] in which the various levels of treatment are coupled and fed back into one another.

Reduced models which retain close connections to the underlying atomistic representation have enjoyed a revival and are currently being developed by many researchers. The aim is to study events which occur on timescales of hundreds of nanoseconds to milliseconds and spatial scales of microns. Modern optical techniques [6] routinely access precisely these timescales and spatial scales. From a theoretical point of view some phenomena in this domain can be addressed with Ginzburg–Landau, and other, expansions of the free energy [7–18]. Free energy methods bias the simulation to study particular events of interest and can be thought of as another way to bridge timescales; however, they fall outside the scope of this review.

In this topical review we focus on the development and application of a coarse grain simulation method that has ready access to events on these scales; coarse grain models are gaining widespread usage in the polymer [19–23] and biophysical communities [24–26]. We begin with some motivating examples of system appropriate to study with these methods. In section 3 we give an overview of existing simulation techniques which access timescales and length scales intermediate between atomistic and mesoscale. We then provide insights into the model building process (sections 3.2, 3.3, and 4) and discuss the consequences arising from the loss of detail (section 5). Next, we look at a few situations in which theoretical predictions can be evaluated by CG simulation methods, and at several situations in which the CG method goes beyond current theoretical and experimental reach to shed some light on novel dynamical phenomena. Lastly, we give some perspectives on future directions for research using CG models.
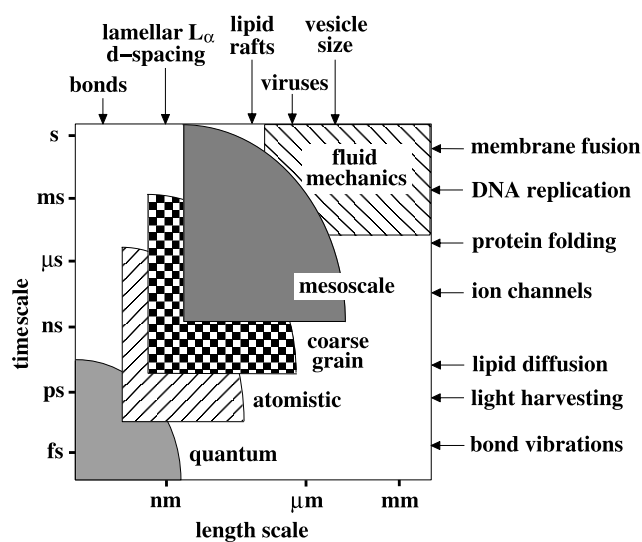
Figure 1. A schematic diagram of temporal and spatial scales accessible by simulation techniques. Also indicated are some characteristic membrane structures and events.

2. Challenges

There are many phenomena that lie within the mesoscopic spatio-temporal scale which may eventually be explored with coarse grain (CG) methods. In a biological context, examples of such phenomena are protein–protein interactions, lipid–protein interactions, and membrane–membrane interactions. Events that fall into these categories include antimicrobial attack on membranes and membrane fusion. From a materials perspective, the optimal design of nanosyringes which penetrate membranes is of interest, as well as the design and properties of artificial polymer based membranes which can act as controlled release vesicles for drug delivery. These are discussed below.

To understand the biological function of lipids, their physical properties must be studied in the context of membranes composed of lipid/protein mixtures. Membrane lipid composition varies widely over different organelle membranes, within a single membrane, and even across leaflets of the same bilayer membrane. These differences in membrane composition range throughout the whole spectrum of living organisms from protozoans to higher organisms such as mammals. For example, the transbilayer lipid distribution is symmetrical in the endoplasmic reticulum of mammalian cells, while it is markedly asymmetrical in the plasma membrane [27]. In the plasma membrane the majority of sphingolipids are found in the outer leaflet while most of the phosphatidylserine and phosphatidylethanolamine lipids are found in the cytosolic leaflet. Local variations in the physical properties of bilayers allow for membrane deformation and facilitate vesicle budding and fusion [28]. Proteins can also stimulate lipid exchange between membranes by bringing them into contact [29]. It is thought that hydrophobic matching between the protein and its matrix is essential for protein function [30]. An understanding of these processes at a mesoscopic or atomic level is currently lacking. An example of a protein assembly which brings membranes into contact is given in section 6.4.

The interaction between membranes can be accounted for by the van der Waals and electric double-layer forces which comprise the Derjaguin–Landau–Verwey–Overbeek (DVLO) theory of colloid science and by the entropic forces due to the overlap of thermally excited surface

modes [8]. Recent results [31] show that the concept of elastic deformation is relevant on lengths comparable to and even less than the bilayer thickness, involving a broad spectrum of collective modes which contribute to the forces between lipid bilayers. X-ray diffraction [32] analysis of bilayers subjected to known osmotic pressures provides information on the magnitude of both repulsive and attractive forces that exist between phospholipid and glycolipid membranes. Atomic force microscopy [33] is also a useful probe of repulsive forces. In section 6.1 coarse grain (CG) and united-atom simulation results on membrane fluctuation modes will be presented.

Experimental studies over the years have shown that vesicles can be formed from organic superamphiphiles such as block copolymers [34, 35]; diblock copolymers in particular have an architecture similar to that of natural lipids. Many biological membrane processes such as protein integration, fusion, DNA encapsulation, and compatibility can be reliably mimicked by synthetic polymer vesicles. The overall copolymer molecular weight is considerably larger (3–20 kDa) than that of their natural lipid membrane counterparts (<1 kDa) [36]. In addition, the hydrophilic/hydrophobic ratio can be selected with ease. One striking feature of polymersomes is that they are hyperthick compared to phospholipid bilayers. The hydrophobic core thickness of this class of vesicles ranges approximately from 8 to 21 nm [37]. Block copolymers have the intrinsic ability to self-organize into membranes and offer fundamental insight into natural design principles for biomembranes. Despite a vast variety of experimental studies, the microscopic details of polymersomes are not understood in detail. Unusually large system sizes (consisting typically of $>10^6$ atoms) makes this task computationally expensive. While current computational resources allows for pre-assembled study of such large systems, it becomes impractical to study dynamical phenomena (for example self-assembly of polymersomes) which occurs typically on a multi-nanosecond to microsecond timescale. Existing simulation studies of block copolymers have been mostly carried out using arbitrary potentials. For example dissipative particle dynamics (DPD) and discontinuous molecular dynamics (DMD) have been used to study the self-assembly of block copolymers by micro-phase separation [38, 39]. The coarse grain approach presented in section 6.3 has proven to be effective and reliable in studying specific phenomena in this area— quantitative comparison with experiments is possible which provides microscopic insight into the polymersome properties.

Membrane channels, pores, and transporters provide pathways for the transport of atoms or molecules across cellular membranes. Successful attempts at synthesizing and incorporating both naturally occurring and synthetic structures into the membrane to observe and control channel activity have been made by various groups [40]. The idea behind this approach focuses on mimicking channel structure and function to understand the principles that drive their activity. There are several approaches for the synthesis of ion channels which can be classified into two main categories. The first involves transmembrane molecules designed from naturally occurring amino acids such as the LS2 and LS3 ion channels of DeGrado and co-workers [41, 42]. In this case the channels are largely composed of naturally occurring Lys and Ser residues that form alpha helices and are engineered to oligomerize through specific residue interactions. The second approach involves the synthesis of non-naturally occurring compounds such as carbon nanotubes and the incorporation of such molecules into natural or synthetic membranes [43]. An example of this approach involves the use of alternating chirality amino acids which are joined to make rings which can then self-assemble into tubular stacks (peptide nanotubes) that form transmembrane structures [44–47]. The selectivity of this construct can be adjusted for discrimination of specific molecules [48]. The advantage of the synthetic approach lies in the feature that channel occupancy and conductivity could in principle be tuned by modifying the local channel environment [49]. In principle, properties such as

tube polarity, local hydrophilicity, and rigidity would be controlled by means of incorporating functional groups into the synthetic channel [40]. The creation of nanoscale devices such as nanosyringes or nanosensors of controlled functionality comprise a field where theoretical modelling could provide insights into the design strategy; such an approach is presented in section 6.5.

A final example where there is an urgent need for an understanding of the dynamics and structure at the molecular level involves antimicrobial attack on membranes. Antimicrobial peptides are present in many vertebrates and invertebrates and their overall structures can be strikingly similar throughout different organisms [50, 51]. Families of these peptides include magainins, cecropins, defensins, and drosomycins [52]. Novel synthetic antimicrobial mimics show promise as effective alternatives to their natural peptide counterparts [41]. Combinatorial synthesis based on these new targets offers potential for averting resistance build-up and boosts the arsenal for combating pathogens. Little is known about antimicrobial mechanisms of action beyond their ability to permeate membranes, induce leakage, and thereby kill pathogenic cells. In section 6.6 we employ coarse grain simulations to identify a two-stage insertion process whereby amphipathic molecules enter and are subsequently accommodated by a lipid membrane. We find evidence for cooperative action. Study of these systems is beyond the scope of current atomistic molecular dynamics (MD) simulations—for example Shai and Sansom note that mechanisms requiring peptide–peptide interactions at the membrane surface have not been studied with simulations [53].

3. Models

3.1. Previous work

There are many approaches in the literature for increasing the efficiency of fully atomistic simulations [54]. For example, lattice based models have a long history in the simulation community because of their efficiency; the bond fluctuation model introduced by Carmesin and Kremer [55] has found numerous applications including the study of interdiffusion of polymer blends, polymer crystallization in dilute solution, and membrane protein folding [56–58]. Current work in this area includes finite-element mesh methods [59], cellular automata based methods [60], and self-avoiding walks [61].

Conservative evolution is numerically unstable and thus a small time step must be employed. The time step used is determined by the stiffest potentials in the system. The highest frequency motions are typically bond vibrations involving hydrogen. Since these fast motions are approximately decoupled from the rest of the system, they undergo many oscillations on the timescale of the remainder of the system. Hence their interaction with the remainder of the system is roughly governed by their average location, which is at the equilibrium bond length. There are algorithms, such as SHAKE and RATTLE, which constrain these high frequency bonds to remain fixed at their equilibrium extensions, thereby eliminating the stiffest motions and allowing the time step to be increased [62]. Another common procedure for eliminating the stiff bond motion involving hydrogen is lumping hydrogen atoms together with their associated heavy atom into a single united-atom site [63]. If only static information is desired, the high frequency motions involving hydrogen can be reduced by artificially increasing the hydrogen atomic mass.

The numerical instability inherent to conservative dynamics can be mitigated by adding dissipative terms to the system. One of the common procedures (known as the Lax method [64]) for stabilizing a flux-conservative partial differential equation is adding a dissipative term. Moreover, methods have been developed in the simulation community which stabilize long time

step integrators for Newtonian molecular dynamics by using very mild stochastic damping [65]. Dissipation can be accounted for with the Zwanzig–Mori projection operator formalism, which provides an exact procedure for eliminating unimportant variables from the system under study [66]. This method leads to the generalized Langevin equation in which the total force acting on the particles of interest is composed of a coloured noise term and a non-Markovian dissipative term containing a memory function satisfying the fluctuation-dissipation theorem [67]. Approximating the memory function with a delta function yields Brownian dynamics [68].

The solvent is a good candidate for a less detailed treatment because it often plays a spectator role, it accounts for a sizable fraction of the system, and it is very time-consuming to treat in full detail because of electrostatics. ten Wolde and Chandler [69] use a coarse grain Ising-like treatment of water to study hydrophobic polymer collapse. For atomic solvents, Malevanets and Kapral [70] treat the solute–solute and solute–solvent dynamics microscopically, while the solvent–solvent dynamics is treated in a mesoscale manner through multiparticle collisions which are hydrodynamically consistent. The solvent can also be accounted for in an implicit manner. Continuum electrostatic models treat the solute as a low dielectric cavity embedded in a high dielectric medium representing the solvent. The Poisson or Poisson–Boltzmann equation is then solved numerically using either finite-difference or boundary element methods. If these numerical methods are too costly, approximations can be used such as the generalized Born approach [71]. A major effort along these lines is under way in the Brooks group to study the folding and assembly of helical membrane proteins [72].

Flekkøy and Coveney [73] have introduced a procedure for deriving a coarse grained dissipative particle dynamics (DPD) from MD. This is the first work to link DPD to the underlying microscopic dynamics. In DPD the forces between particles have fluctuating, dissipative, and conservative components [74]. Momentum and mass conservation are imposed to produce hydrodynamical behaviour at the macroscopic level. The parametrization method of Groot and Rabone [75] only requires the correct compressibilities and the correct solubilities of the various components into each other. These mutual solubilities are specified with Flory–Huggins χ-parameters [76].

The protein folding community has long been interested in CG models for increasing the efficiency of protein structure predictions. Typically amino acid residues are represented by one or two interaction sites, and the peptide backbone unit is represented as a single site [77, 78]. The force field is parametrized from radial distribution functions computed from the Protein Data Bank (PDB). It seems at first that these data have little importance for determining potentials along folding pathways, and in particular for starting with unfolded sequences. But in fact even though the entire protein is in its folded state in the PDB archive, a particular short amino acid sequence appears in many structures in very different conformations, so short sequences should be sampled in roughly a Boltzmann distribution across all structures [78].

3.2. Reduced model considerations

We now focus on methods and considerations pertaining to the development of reduced models. There are many decisions which must be made, including the nature of the dynamics—conservative or dissipative—and the functional form of the interaction potentials. We touch on some of these choices in what follows and supply detail for systems with which we have experience.

A common motif employed by many simulation methods is lumping groups of atoms together into a single interaction site. We give as examples the CG model of Fukunaga [20], the DPD model of Groot and Rabone [75], and the multiscale method of Goddard [79].

It is important not to overly distort the geometrical shape of the molecules when doing this grouping. As an illustrative example, for amphiphilic molecules the head group size compared to the average tail size normal to its length determines whether micelles or inverse micelles are preferred. Cone shaped molecules such as phosphatidylethanolamine have small head groups and tend to form inverse micelles. Inverted cone shaped molecules such as lysophosphatidylcholine tend to form micelles. Some models use anisotropic interaction sites to capture the underlying shape; one of the simplest is the Gay–Berne potential which is commonly used in liquid crystal simulations. It has been used in a lipid CG model [80] and in a united-residue protein folding model [77]. For large coarse grain site groupings, additional physics is required to describe the system: for example Briels [81] introduces uncrossability constraints into a CG polymer model to prevent unphysical bond crossings.

The electrostatic partial charges also must be considered when choosing the CG grouping. All-atom MD force fields typically have atom-centred partial charges to capture the electron-withdrawing capabilities of certain functional groups. Lumping atoms together into a single interaction site imbues that site with a partial charge which is the sum of all its constituent atomic charges. If this is not satisfactory the interaction sites may have to be reduced in size or have their composition altered. One possibility is to associate several fictitious charges with an interaction site so as to reproduce the correct long range electrostatics. As an example of this we mention the peptide backbone structure. The peptide backbone partial charges give an α-helix its net dipole moment and its hydrogen bonding network. The backbone unit could be modelled as the electrically neutral $-C_\alpha H-CO-NH-$ site (possibly with two fictitious charges) or as two sites, $-CO-$ and $-NH-C_\alpha H-$, with equal positive and negative partial charges. The protein folding community often uses a single, uncharged site [77, 78]. An alternative is to use a multipole expansion to capture the effect of an anisotropic charge distribution. Recently, Groot [82] has incorporated electrostatic interactions into the DPD framework. The electrostatic field is solved locally on a grid, allowing for proper treatment of local inhomogeneities in the electrostatic permittivity.

Parametrization of all-atom and united-atom classical MD force fields is a highly developed, yet still active [83], area of study. These force fields are typically parametrized from a combination of experimental observables and quantum calculations. Reduced models have an additional source to draw upon, namely atomistic simulations. In particular, it has become commonplace for short atomistic simulations to be used to attempt to include fine detail in a statistical (mean field) manner. This is done by appealing to reverse Monte Carlo (MC) simulation techniques [84, 85] to implicitly capture fine structure. For example, the aqueous solvent shell structure around ionic or zwitterionic species involves a complicated hydrogen bonding network. In all cases in the literature it is the radial distribution function (denoted as RDF or g) which is used. However, it should be possible to use c, the Ornstein–Zernike direct correlation function, instead of the full correlation function $h \equiv g - 1$. The advantage of using the direct correlation function to parametrize a non-bonded pair interaction is that it avoids the ambiguity of having oscillations in the tails of the various interaction potentials which cancel each other out (and hence need not exist). The full correlation function is conceptually and pragmatically difficult to relate to the effective non-bonded potential because of many-body effects [20].

Clearly there are a plethora of options in designing reduced models. Many of these choices necessitate writing new simulation software to implement unusual or novel Hamiltonians. Even something as simple as the multibody hydrogen bonding term introduced by Kolinski and Skolnick [78] to encourage cooperativity in protein folding would require modification of standard simulation code. The efficiency gain intrinsic to the reduced model is hindered if the simulation algorithm does not parallelize efficiently. To take advantage of the superior parallel

performance of established simulation codes such as NAMD [86], the reduced model should look similar in structure to atomistic ones.

Let us pause for a moment to ask whether it is worth going to all this trouble to determine the force field. Historically CG models have used arbitrary force fields which take little effort to construct [87]. If the goal of the modelling study is to explain experimental trends in a generic fashion, this may be sufficient. The early efforts by Larson in exploring CG amphiphile systems are exemplary in this regard [88–90]. However, to be able to quantitatively compare with experiment, an accurate force field is needed. Paul describes a procedure for mapping atomistically detailed polymer models onto the bond fluctuation model which incorporates both static and kinetic information. The purpose is to transfer information about a specific polymer into a simpler model to study its large scale and long time properties [19, 91]. Outside of the polymer community, however, Scott points out in a recent review that existing CG models 'suffer from a lack of connection to atomistic interactions, which must ultimately be responsible for phase separation and domain formation' [92]. Our experimental collaborators in particular have enough data to justify building accurate models as a complement to their studies [93, 94, 41].

3.3. Hierarchical strategy for model building

A hierarchical approach is now described for determining the force field. The general strategy in a system with several components is to separately treat the hydrophobic and hydrophilic components, and then to combine them. Hydrophobic components are usually involved in non-specific interactions and hence it should be possible to develop a model for them which is suitable for a wide range of systems.

To begin we consider the hydrophobic parts of the system of interest separately. For each type of CG hydrophobic unit, the single-component bulk liquid is subjected to brief atomistic simulations to ascertain the nature of the intramolecular potentials and if needed the bulk density. By intramolecular potentials we mean the effective potentials between groups of atoms corresponding to the CG sites. In the polyethylene model of Fukunaga [20] the bond and bend potentials are determined by taking the logarithm of the corresponding canonical distribution functions calculated from atomistic simulations. This requires that one forego simple functional forms for these potentials. In both our experience [23] and in the Fukunaga model the target bond potentials have two minima corresponding to the bent and extended configurations. This shape arises from correlations with other degrees of freedom. Fully reproducing the distribution in the CG representation changes the nature of the barrier between the minima from having a dynamical origin to having only a statistical one; for simplicity we choose to approximate the distribution as unimodal because we are not concerned with this level of detail. For the intermolecular potential, which can also be derived from atomistic canonical distributions [21], a soft (CG interaction sites always have softer potentials than their all-atom counterparts because the constituent atomic sites become smeared out) Lennard-Jones form is preferred for its transferability. The two parameters, namely the contact distance and the well depth, are tuned to reproduce the target bulk density and surface tension, which are obtained from experiment or from theoretical estimates [95]. One can check, *a posteriori*, the quality of the radial distribution functions; we have found the agreement to be excellent [23]. The reason we use surface tension, and its condensed phase counterpart interfacial tension, as a target observable is because we typically wish to simulate systems containing amphiphilic species. It is felt that interfaces are of crucial importance to model accurately in such systems.

While the hydrophobic tails can be studied in the bulk, hydrophilic entities must be considered in an aqueous environment to properly model them. For example, poly(ethylene
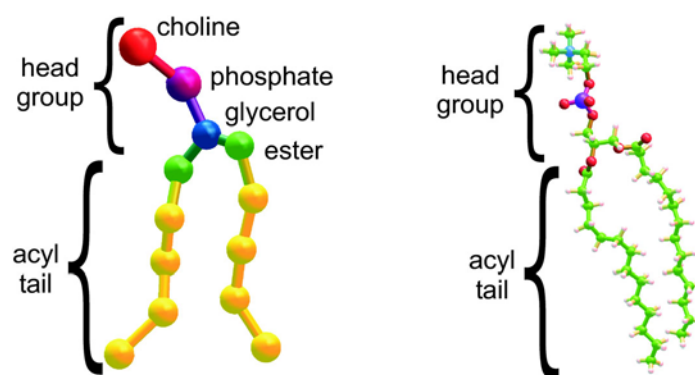
Figure 2. The 13-site model of dimyristoylphosphatidylcholine (DMPC). The choline and phosphate sites carry positive and negative electrostatic charges, respectively, of equal magnitude. The all-atom version is also shown.

oxide) adopts an all-*cis* conformation in vacuum, but an all-*trans* conformation is preferred in water. The representation of water in reduced models varies widely; we consider for what follows the flexible choice of a dual identity. On the one hand, radial distribution functions between aqueous hydrophilic groups, obtained from atomistic simulations, implicitly include water through solvation shell structure. On the other hand, it is desirable to have an explicit representation of water. This is for two reasons. Firstly an attractive well in the potential between explicit waters allows the water to maintain a subcritical interface—necessary for studies of Langmuir monolayers for example. Secondly, the explicit water serves as a momentum carrier in MD simulations, the importance of which is discussed in section 5.2. For these purposes a soft Lennard-Jones fluid is sufficient to represent the explicit part of the solvent [26]. The Lennard-Jones parameters are chosen to have the correct bulk density and air/liquid surface tension at room temperature.

For interactions among the hydrophilic groups, greater emphasis is placed on the radial distribution functions (RDFs) as a way to capture detailed structure in a statistical manner. Depending on the interest one can tune the hydrophilic interactions for specific environments to reflect the explicit interactions such as local hydrogen bonding and solvation shell structure [26]. As a consequence, the hydrophilic components may have to be modified for use in other settings.

Next, the interfacial components must be modelled. A lack of statistics hinders the construction of an accurate model: for example in an atomistic simulation of poly(ethylene oxide)–poly(ethylethylene) (PEO–PEE) diblock copolymer, only one bead per diblock chain is an interfacial unit. A similar procedure to that for hydrophilic groups is used.

Lastly, the cross-terms between hydrophilic and hydrophobic groups must be determined. If possible this should be done on the basis of interfacial tension. For example, the hydrocarbon–water interaction potential well depth can be chosen so as to reproduce the interfacial tension of roughly 50 dyn cm^{-1}.

In the following we mention the parametrization of the phospholipid dimyristoylphos-phatidylcholine (DMPC) and the PEO–PEE diblock copolymer. The DMPC molecule is coarse grained using 13 sites to represent the 118 atoms as shown in figure 2. An all-atom simulation [96] of an equilibrated DMPC bilayer in the L_α phase is used to parametrize the CG model. The CG system that we will calibrate is also prepared as a bilayer so that we are treating the same thermodynamic phase. The lipid head groups are coarse grained into a
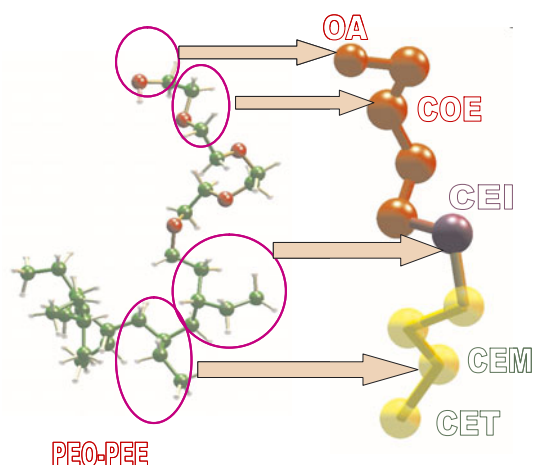
Figure 3. Mapping of a fully atomistic PEO–PEE diblock copolymer (left panel) onto a coarse grain model (right panel). The EO monomer –CH_2–O–CH_2– and the EE monomer –CH_2–CH(CH_2–CH_3)– are represented by the coarse grain units COE and CEM, respectively. The COE choice is preferred over an ethylether monomer unit –CH_2–CH_2–O– due to symmetry. CEI denotes the interfacial unit –CH_2–CH(CH_2–CH_3)–CH_2–, while the end groups, namely tertiary butyl and CH_2–OH, are represented by CET and OA, respectively.

positively charged choline site, a negatively charged phosphate site, a glycerol site, and two ester sites which have the two alkanoyl tails attached to them (see figure 2). All combinations of non-bonded pairwise interactions among these head groups are modelled with tabulated effective potentials which aim to reproduce the radial distribution functions from the appropriately grouped all-atom simulation data (see Shelley [26] for further detail). A similarly constructed coarse grain model of the PEO–PEE diblock copolymer is pictorially shown in figure 3. In this representation, each monomer constituting the polymer is represented by a single spherical coarse grain unit. Both the hydrophobic and hydrophilic components are just linear monomer repeats, making the parametrization easier. A combination of experimental (density, surface tension) and atomistic simulation (RDFs) data is used to construct the CG model.

4. Parameter optimization

Once the target data and the model have been established, the optimal parameter set must be determined. This procedure is numerically intensive and time-consuming but is largely devoid of physics. A representative selection of optimization strategies are presented below.

The simplest and slowest method is the fully automated simplex optimization procedure introduced by Müller-Plathe and co-workers [97]. A proviso is that automatic, or 'blind', parametrization schemes might give unphysical results due to offsetting effects; see the discussion by Müller-Plathe for some examples [21]. An extremely sophisticated optimization strategy which also *only* uses function values is the APPSPACK package from Sandia National Laboratories [98]. This is an asynchronous and fault tolerant parallel pattern search method which has been specifically designed for problems characterized by expensive function evaluation (typically complex simulations that take hours to run).

For the specific problem of using a tabulated potential to reproduce a target radial distribution function, Müller-Plathe [21] suggests beginning with the potential $V_0(r)$ which

is the potential of mean force obtained by Boltzmann inversion of the target RDF, and subsequently iterating according to

$$V_{n+1}(r) = V_n(r) + kT \ln \frac{\mathrm{RDF}_n(r)}{\mathrm{RDF}_{\mathrm{target}}(r)}. \tag{1}$$

Fewer than ten iterations are normally required for convergence.

Finally, we present a gradient based optimization method due to Lyubartsev and Laaksonen [84] which can be used to compute the full matrix of first partial derivatives, relating the changes in input parameters to the changes in observables, from a single simulation. We wish to establish the change in the observable A caused by a change in the parameter a. This relation allows for the parameter adjustment to be made optimally to first order. We assume the Hamiltonian

$$H = \frac{P^2}{2M} + V(R; a) \tag{2}$$

depends upon a parameter a, where the first term in equation (2) is the kinetic energy of the system and the second term is the potential energy. For the observable $A \equiv A(R)$ depending only on the coordinates, its expectation value in the canonical ensemble is given by

$$\langle A \rangle = \frac{\int \mathrm{d}R \, A \mathrm{e}^{-\beta H}}{\int \mathrm{d}R \, \mathrm{e}^{-\beta H}} \tag{3}$$

where β is the inverse of the product of Boltzmann's constant and the temperature, so

$$\frac{\partial \langle A \rangle}{\partial a} = -\beta \left[\left\langle A \frac{\partial H}{\partial a} \right\rangle - \langle A \rangle \left\langle \frac{\partial H}{\partial a} \right\rangle \right]. \tag{4}$$

This is the fundamental relation which links the change in input parameter to the change in output observable.

5. Consequences arising from the loss of detail

There are several consequences of moving from a fully atomistic description to a coarse grained one [99]. It is well known that all models which use *effective* pair potentials, including condensed phase all-atom (AA), united-atom (UA), and coarse grain (CG) force fields, are thermodynamically inconsistent [100, 22]. Louis [100] concludes that, at best, a force field which uses effective pair potentials can be chosen to perform well for some particular physical properties of interest. In this respect AA and CG models are on the same footing. However, CG models usually make use of atomic-level pair correlation functions, either from atomistic simulations [84] or from experiment [101], as data to parametrize against. This strategy has the advantage that detailed structural information is incorporated into the CG model, but suffers from a loss of transferability; since the radial distribution function incorporates temperature, density, composition, and other dependences into the effective pair interaction, the resulting force field can have a severely limited range of applicability [63]. In particular the phospholipid parametrization described in section 3.3 builds specific L_α bilayer structure directly into the force field. Furthermore, the derived force field is only valid for a small temperature range as discussed in section 5.1. This is part of the trade-off in moving to a more efficient simulation method; generality is sacrificed. However, the situation is not as limiting as it first appears. Only the lipid head group–head group interaction potentials contain explicit bilayer information since these were the only potentials that were tabulated to reproduce the thermodynamic phase-specific atomistic radial distribution function data. The rest of the interaction potentials are general. Furthermore, the enthalpic lipid tail and entropic changes which occur when the
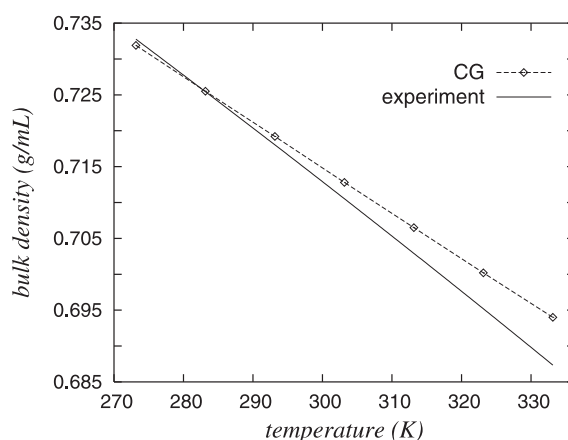
Figure 4. Experimental and CG density of nonane as a function of temperature. The experimental data are in the form of an analytic fit by Rudek [103].

lipid/water system is in a different phase can partially override the structure inherent in the non-bonded potentials. Ongoing studies using this L_α bilayer derived force field include Langmuir monolayers and inverse hexagonal phases [102]; the results (e.g. the surface tension of Langmuir monolayers) are encouraging and agree qualitatively with experiments.

5.1. Temperature dependence

We turn briefly to show the temperature dependence of the density of nonane from one of our alkane model systems [23]. The CG parametrization only made use of data at a temperature of 303 K. Nonetheless, the form of the intermolecular potential leads us to expect roughly the correct temperature dependence because condensed phase Lennard-Jones well depths are typically independent of temperature. For the range $273\,\mathrm{K} < T < 333\,\mathrm{K}$, the density of nonane has a regression-fitted slope of $-7.565 \times 10^{-4}\,\mathrm{g\,cm^{-3}\,K^{-1}}$ for the experimental data which are in the form of an analytic fit by Rudek [103], and a slope of $-6.32 \times 10^{-4}\,\mathrm{g\,cm^{-3}\,K^{-1}}$ for the CG model, an error of 16% (see figure 4). The current force field is valid in a narrow temperature range at room and physiological temperatures. In cases where a greater temperature range is desired, such as in polymer science, the parametrization can be undertaken, separately, at different temperatures and the resulting CG potentials can be fitted to include temperature dependence [20].

5.2. Efficiency over atomistic simulations

Work on the current CG model began by using MC as the sampling technique with a simple move set [26, 104]. Large scale organization and healing were observed to be slow. For example, inverse hexagonal self-assembly did not show global structure over the course of an MC simulation, and defects in the self-assembly of a lipid bilayer did not heal over the length of the simulation [104]. This problem would be alleviated by using a more sophisticated MC move set [105, 106]. Instead, MD was appraised as an alternative simulation technique. The use of MD was observed to be very efficient. Besides the cooperative global moves which occur naturally in MD, the explicit water particles act as momentum carriers and allow for material to flow in the system in a hydrodynamically consistent manner that aids global rearrangements. The efficiency of the CG MD method over all-atom MD approaches will now be described.
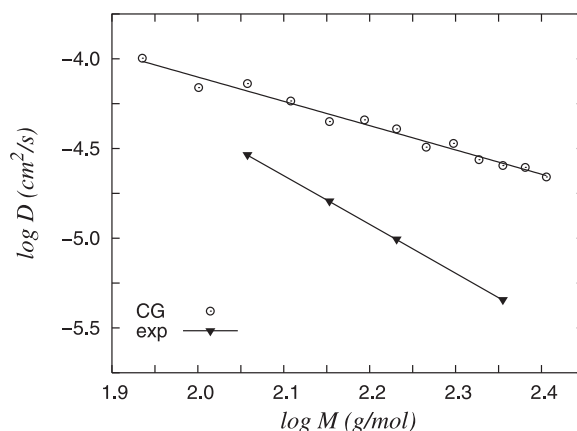
Figure 5. Experimental [109] and CG diffusion coefficients of linear alkanes at 303 K. Both sets of data are linear on a log–log scale, with a slope of -2.72 for the experimental data and -1.35 for the CG data.

The softer interaction potentials allow the use of a propagation time step that is one order of magnitude larger. The reduced number of interaction sites and potentials between them yield another speed-up, by two orders of magnitude. In the case of the phospholipid DMPC [26], the CG model consists of 13 sites and 24 internal potentials (12 bonds and 12 bends). The all-atom CHARMM DMPC encompasses 118 atoms and 971 internal potentials (117 bonds, 226 bends, 315 torsions, and 313 one-fours). A further efficiency gain by two orders of magnitude comes from enhanced diffusion of the lipid species, for example in the plane of a bilayer or Langmuir monolayer. This is a result of the soft interaction potentials and the lack of an explicit hydrogen bonding network at the interface between lipid head groups and water. We have quantified this diffusional speed-up [107, 108, 23] as follows.

5.3. Diffusional timescales

The use of soft potentials and a reduced number of interaction sites make it worthwhile to get an idea of the effective timescales that are being accessed by the CG models. No CG model to date has been parametrized using dynamical data [21], and it is well known that parametrization using structural and thermodynamic properties results in diffusion coefficients which are too high [80, 108]. The soft intermolecular potentials which are responsible for the inflated diffusion are also responsible for being able to use a larger time step in integrating the equations of motion, and are a consequence of the reduced representation. Nonetheless, Whitehead [80] proposes using a CG model to study the diffusion of small molecules within a bilayer membrane. This could be accomplished by constructing a calibration curve between the CG diffusion coefficients and those obtained either from an AA membrane simulation or from experiment [80].

Experimental results establish that the diffusion coefficients of single-component alkane melts are linear on a log–log scale when plotted against the molar mass [109]. The CG alkane data from our parametrization [23] are also linear on this scale, as shown in figure 5. The data in figure 5 can be used to gain a rough idea of the relationship between the CG simulation time and the actual time.

For amphiphilic systems the diffusional timescale difference between atomistic and CG simulations can be much greater. The two-dimensional lateral diffusion constant for the L_α
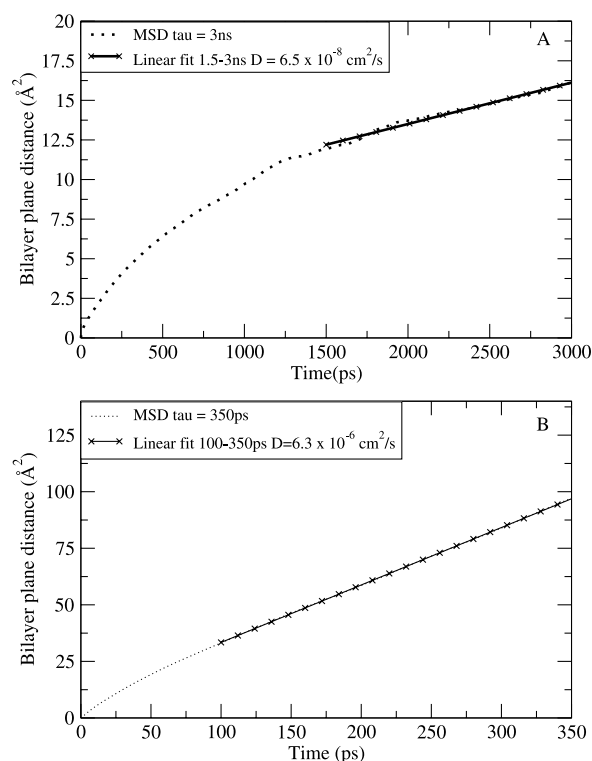
Figure 6. The two-dimensional mean square displacement for a 10 ns all-atom DMPC simulation (A) and an 800 ps CG-DMPC simulation (B). The fits are represented by the lines with crosses.

phase of DMPC in the plane of the bilayer is $6.5 \times 10^{-8}\,\text{cm}^2\,\text{s}^{-1}$ for an all-atom simulation [110] and $6.3 \times 10^{-6}\,\text{cm}^2\,\text{s}^{-1}$ for the CG model [108]. These data are shown in figure 6.

5.4. Rotational timescales

The rotational self-diffusion coefficients for an atomistic DMPC lipid bilayer simulation were determined previously [110] and are used here to compare to its CG counterpart [108]. Figure 7 shows the plot of the mean square displacement of the individual vectors and the curves from which the diffusion coefficients are calculated.

For this calculation a molecular fixed reference frame is required. The principal axes of the moment of inertia tensor (MIT) allow the rotations of the molecule to be quantified (see figure 8). We project the xy components of the MIT onto the xy plane to examine the overall molecular rotation, and the projection of the z component of the MIT onto the xy plane is used to examine the overall wobble. In addition, we investigate the molecular rotation using the different vectors shown in figure 8: the PN vector links the phosphate unit to the choline (tetramethyl ammonia) unit (see figure 2) while the SM (ST) vector is drawn from a hydrocarbon (terminal hydrocarbon) unit in one tail to its counterpart in the other tail.

The PN vector in the CG model rotates much more freely than that of the AA simulation. In the AA simulation the zwitterionic head groups form a hydrogen bonding network with both water molecules and other lipids. This hydrogen bonding network must be broken in order for the head groups to rotate. In the CG model however, the detailed hydrogen bonding network between water and head group as well as between head groups has been captured in
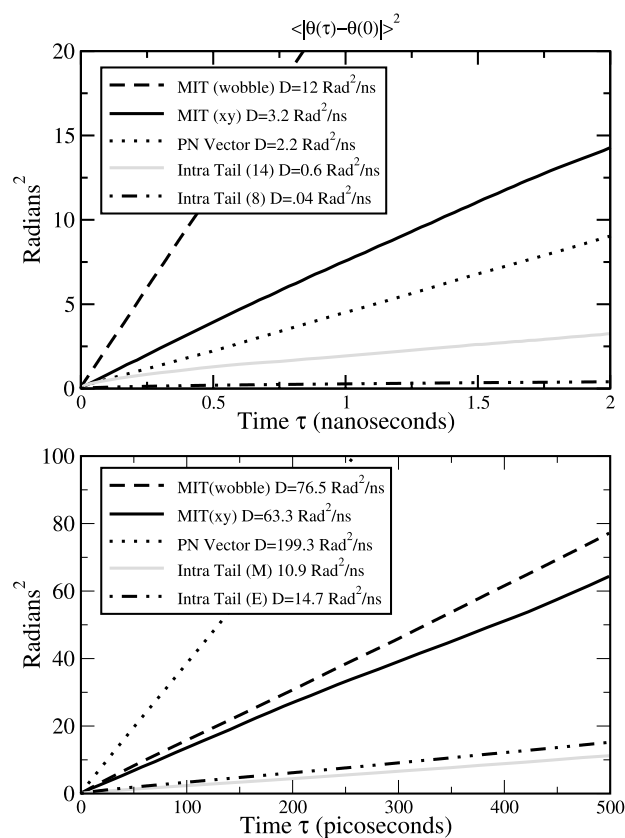
Figure 7. Comparison of the rotational diffusion between an all-atom simulation (top) and the CG lipid simulation (bottom). The plots are the mean squared displacements of the vectors illustrated in figure 8.

a statistical manner by the use of effective potentials. The resulting force field therefore has reduced dynamical significance.

The two tail vector diffusions are roughly equal for the CG model while those for the AA simulation differ by about an order of magnitude. This is not surprising because in the CG model there are only four sites in the tail while the AA model has fourteen carbon atoms with their respective hydrogen atoms. In the AA model the long hydrocarbon tails tend to tangle and interact extensively making the rotations of the tails very slow when compared to the rotations of the rest of the molecule. In the CG model, the tail and molecular construct rotate as one unit.

It is evident from the discussion that it is not possible to capture all the properties of the system under study with a coarse grain construct. This is, however, precisely the point of using a reduced representation model; the aim is to capture the major details that will influence the mesoscale behaviour of the system of interest.

6. Applications

We begin by discussing some recent simulation work which is motivated by experimental and theoretical results on entropic forces in amphiphilic systems. We then proceed to illustrate the range of applicability of the current CG method by presenting some of our recent results.
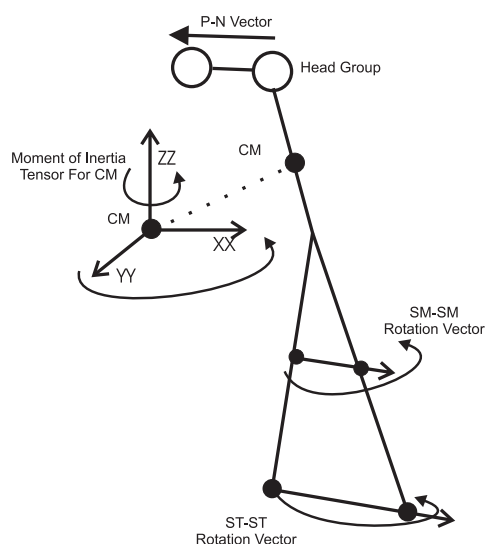
Figure 8. An illustration of the various vectors chosen to study rotational dynamics of DMPC. The vectors are defined and described in the text.

6.1. Fluctuation modes

The forces between fluid amphiphilic surfaces arise from both entropic and enthalpic factors. The enthalpic contributions arise from the two forces which comprise the Derjaguin–Landau–Verwey–Overbeek (DVLO) theory of colloid science. These are the attractive van der Waals and repulsive electric double-layer forces, the latter being present only for charged amphiphiles. The entropic contributions [8] are repulsive and arise from the overlap of thermally excited surface modes. Two of these are the undulatory and peristaltic (or squeezing) modes. These two modes are most easily visualized in the case of a hydrated bilayer. On locally orienting the bilayer to lie in the xy plane, the position of the two bilayer leaflets at a particular xy location can be taken to be h_ℓ and h_u (e.g. these locations could be the centre of mass of the head groups or the centre of mass of the amphiphiles). The undulatory mode is given by the fluctuations in $h_\ell + h_u$ while the peristaltic mode is given by the fluctuations in $h_\ell - h_u$ as a function of x and y. For uncharged amphiphiles the dominant interactions between amphiphilic surfaces at distances greater than 1 nm are due to the repulsive undulatory and attractive van der Waals forces [11]. Both scale as the inverse cubic distance between surfaces. The van der Waals pressure scales as [8]

$$P_{\text{vdW}} \propto -\frac{A}{6\pi D^3} \tag{5}$$

where A is a constant and D is the separation between surfaces. The undulatory pressure scales as [11]

$$P_{\text{und}} \propto \frac{1}{\beta^2 K_b D^3} \tag{6}$$

where K_b is the elastic bending modulus. We will focus on uncharged amphiphiles for the remainder of this section, but wish to point out that recent simulation work [111] has obtained results which differ qualitatively from the electrostatic predictions of DVLO theory. Moreover, it is thought [8] that electrostatic charges suppress undulatory and other fluctuations.

Simulations are beginning to evaluate the validity of these scaling predictions at the microscopic level. However, recent work has focused on the thermal fluctuations within a single surface. The best known example of these intra-surface fluctuations is capillary waves [112], which in interfacial monolayers are predicted to broaden the interface width σ due to thermal excitations as

$$\sigma^2 = \frac{1}{\beta 4\pi^2 \gamma} \int_0^\infty dq \, \frac{q}{q^2 + \kappa^2} \tag{7}$$

where q is the wavenumber, γ is the surface tension, and κ accounts for the presence of the gravitational field. This expression diverges logarithmically with system size and an upper cut-off must be invoked. Typically this cut-off is taken to be the bulk correlation length of the liquid. Logarithmic divergence is weak; for a typical system [7], a surface of extent $L = 100$ Å has a root mean square (rms) fluctuation of about 1.5 Å, while one with $L = 1$ cm has an rms fluctuation of only about 7.5 Å.

Since the capillary fluctuations are small, simulations have studied lipid bilayers in the lamellar phase, where the fluctuations are more pronounced. In this case the main entropic fluctuation force is due to the bending of the bilayer. The mean square height fluctuation grows algebraically with the system size [7]

$$\sigma^2 \propto \frac{T}{K_b} L^2 \tag{8}$$

where T is the temperature, K_b is the bending modulus of the bilayer, and L is the planar spatial extent of the system. This prediction of much faster divergence is accessible to and has been tested by the simulation community using both CG and united-atom models [113–116]. The elegant study of Marrink [115] examines the role of lateral tension on the undulations which has also been addressed experimentally [117]. The recent CG study of den Otter [118] confirms the quadratic form of equation (8) for equilibrium MD simulations, but using non-equilibrium methods to go beyond thermally accessible amplitudes exposes a clear deviation from the theory. In addition to bending fluctuations, bilayers undergo peristaltic fluctuations. The simulations of Marrink [115] clearly show the expected long wavelength suppression of the peristaltic modes since these fluctuations cannot exceed the mean width of the bilayer.

6.2. Self-assembly process of a monolayer

Amphiphilic self-assembly is well established for generic model systems using coarse grain simulation techniques [119–121, 87, 122–125] and is the subject of recent atomistic studies [126–128]. We have studied many self-assembly processes from uniformly random initial conditions, including bilayers [26], monolayers [129], and inverted hexagonal phases [104].

Here we present the results for a monolayer self-assembly process which was studied by randomly placing lipid and water molecules in a slab geometry with two air/liquid interfaces (figure 9(A)). The system self-assembles within 300 ps into two Langmuir monolayers and a cylindrical micelle in the bulk water region (figure 9(B)). The micelle drifts towards and fuses with one of the monolayers [108] within 1.5 ns, giving a final configuration of two unequally populated monolayers (figure 9(C)). The entire process is captured in figure 10, which shows the time evolution of the lipid head group density projected normal to the air/water interface.

Initially, the inhomogeneities that are present in the random initial placement of molecules give rise to local organization as the lipid tails try to remove their contacts with water. In very short order these local aggregates accumulate either in a micelle in the bulk water region or as Langmuir monolayers at either of the two air/water interfaces (figure 9(B)). Although
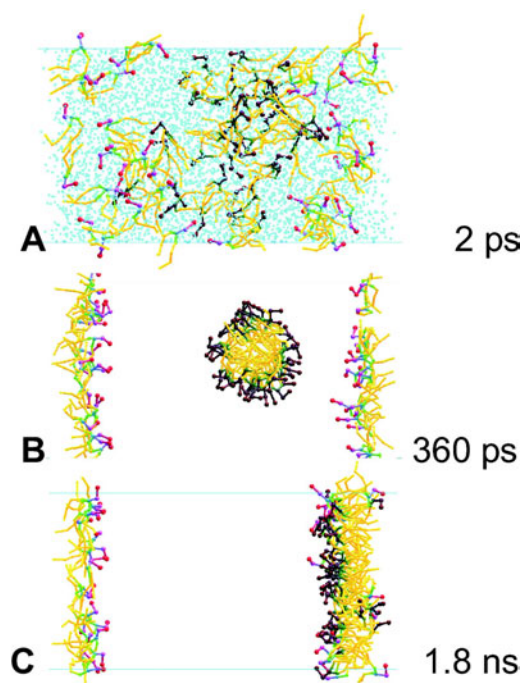
Figure 9. Langmuir monolayer self-assembly. A random slab initial condition (panel (A)) consisting of 80 DMPC lipids and 5000 water sites organizes into two Langmuir monolayers and a cylindrical micelle (panel (B)). The micelle then fuses with one of the monolayers (panel (C)). Water is omitted from panels (B) and (C) for clarity. The micellar lipids of panel (B) are shown with dark head groups in all three panels.

the precise number of lipids in each of these three entities will vary with the particular random placement initially chosen, this tripartite segregation was always observed over several simulations involving differing numbers of lipids and using different random number seeds.

The micelle could initially find itself far removed from the interfacial monolayer in a bulk water environment, or it could form close enough to the interface to immediately interact with one of the interfacial monolayers. In the former case the micelle will diffuse as an entity in bulk water—since it sees an isotropic bulk water environment it will diffuse randomly until at some point it drifts close enough to an interface to interact with one of the monolayers. This interaction can be thought of, at far enough separation, as the interaction between two amphiphilic surfaces [8]. In the case of the zwitterionic DMPC lipid there is no electric 'double layer' and it is observed that the micelle eventually fuses with the interfacial monolayer (figure 11) [8]. The processes of both micelle diffusion and fusion with the monolayer are long timescale events which are well suited to study by the CG approach.

6.3. Diblock copolymer self-assembly

The hydrophilic/hydrophobic ratio greatly affects the morphology of a diblock copolymer system. For a simple lipid or diblock copolymer in an aqueous solution, the time averaged molecular shape determines the morphology of the system. For example, cylinder, wedge, or cone shapes lead to the formation of membrane, rod-like, or spherical morphologies,
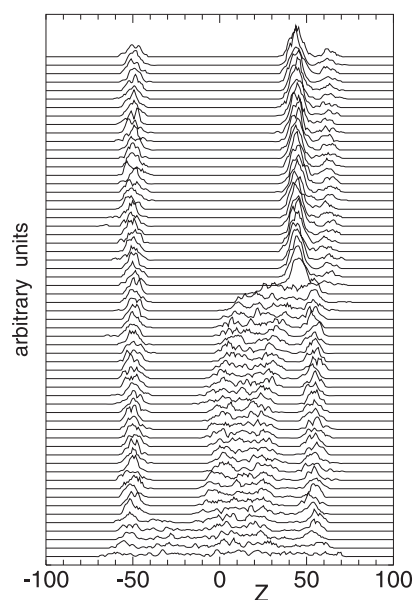
Figure 10. Evolution of lipid head group density throughout the self-assembly simulation. The head group electron density is projected onto the axis normal to the air/water interface at 60 equally spaced intervals over the 2 ns simulation. The system quickly assembles into two interfacial monolayers and a micelle in the bulk water environment. This micelle then diffuses towards and fuses with one of the Langmuir monolayers. The formation of a partial outer leaflet should be noted.

respectively [130]. For illustrative purposes we select a diblock system with 45% hydrophilic content. The initial configuration and snapshots obtained during the self-assembly process are presented in figure 12. Copolymers start self-assembling spontaneously through the clustering of hydrophobic groups. The cluster sizes increase with time as shown in figure 12(C). The hydrophilic segments, being relatively small, are unable to prevent the hydrophobic chains from being exposed to water. This motivates rapid self-assembly among the hydrophobic segments in a direction that minimizes their exposure to water. The two separate clusters gradually merge and form a single continuous worm-like micelle after the readjustments, as shown in figures 12(E) and 12(F).

Care should be taken in conducting such self-assembly studies. The periodic boundary conditions and small simulation cell size may result in the stabilization of metastable structures [131]. Furthermore, the initial dynamics for the MD self-assembly simulations should not be considered in detail. The instantaneous pressure is extremely high due to the large hydrocarbon–water interface and the force field was developed under equilibrium conditions. However, the gross features of the initial dynamics are correct. The dominant effect is for the system to minimize the extent of the hydrophilic/hydrophobic interface.

6.4. Membrane contact induced by a transmembrane peptide

The typical picture of the bilayer-spanning part of a transmembrane peptide is of a hydrophobic alpha helix with caps that preferentially associate with the interfacial lipid head group–water region. Membrane lipids also have a hydrophobic region consisting of the conjunction of their acyl tails. Lipid bilayers are more easily deformed than alpha helical transmembrane
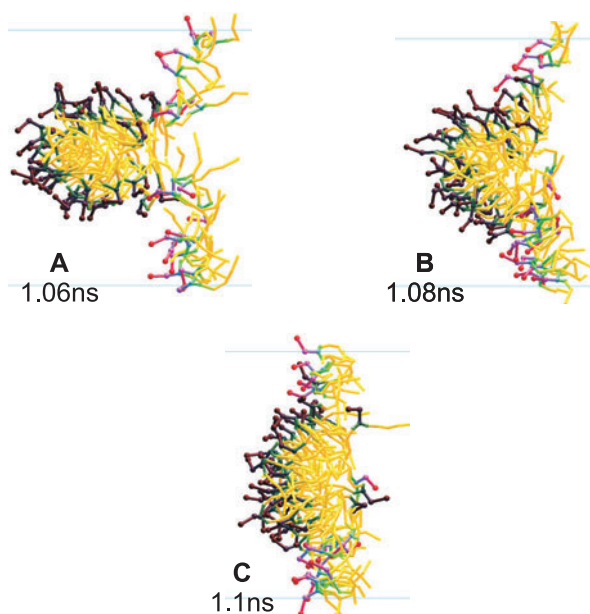
Figure 11. The fusion of the micelle with the monolayer. In panel (A) the monolayer lipid head groups evacuate the region near the incoming micelle. The micellar lipids closest to the monolayer, which are initially oriented in the opposite direction to the monolayer lipids, also have their head groups removed from this region. Panel (B) shows a snapshot shortly after fusion has begun. Notice that some lipids are ejected towards the outer surface during the collision. Panel (C) shows the micelle close to the end of the fusion event. Most head groups have aligned facing the water, while some lipids form a partial outer leaflet. The shading is as in figure 9.
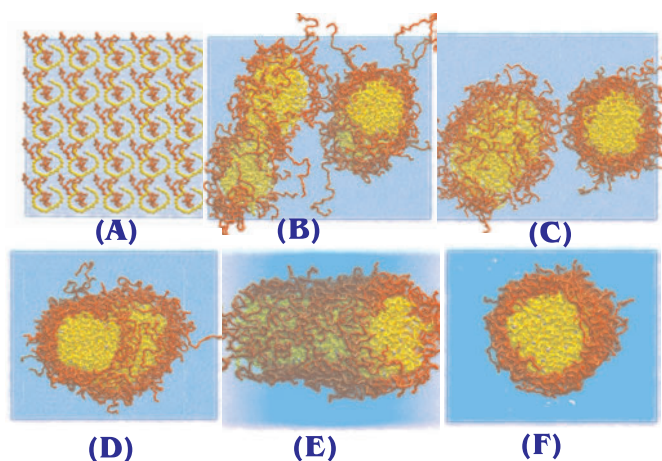

Figure 12. Self-assembly of a worm-like micelle as observed in CG simulations. Simulations are started from a lattice configuration (A) with 100 $EO_{40}EE_{37}$ diblock copolymers in $20\,000$ CG water sites. Aggregation of the hydrophobic blocks into two clusters (B), (C) is followed by their merger (d) into a worm-like micelle which spans the simulation unit cell, shown from two viewpoints (E), (F). The EO monomers are shaded dark; the light EE monomers form the core of the micelle.

proteins [132], and the assumption is made that the bilayer deforms to match the hydrophobic length of the protein [133], leaving the protein virtually unchanged. Theoretical considerations
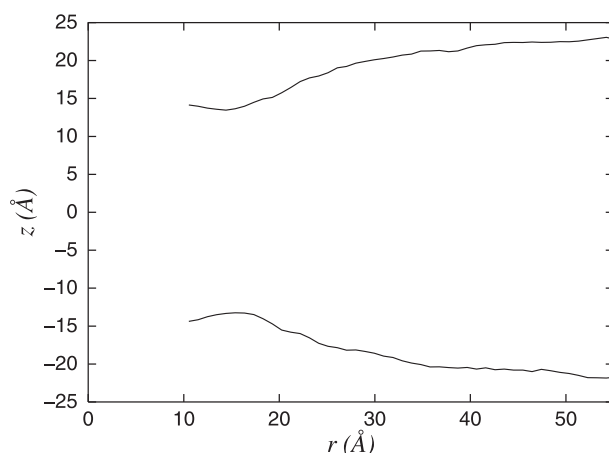
Figure 13. The extent of the lipid meniscus formed around the transbilayer peptide. The radial distance r of lipids from the peptide is plotted against the distance z of lipids from the peptide in the direction normal to the bilayer plane. The two leaflets are shown by positive and negative values. The lipid position is taken to be the centre of mass of the head group. The peptide position is taken as its centre of mass.

point to a range of effects that contribute to the free energy in the presence of such a peptide inclusion. These consist of elastic acyl chain stretching/compression, surface tension terms accounting for the average interfacial area per molecule, curvature contributions from the formation of a meniscus around the inclusion, and tilt modulus of the acyl chains [13, 12, 14, 134, 135].

For a short, hydrophobically mismatched peptide assembly we observe meniscus formation when the peptide is incorporated into the membrane [136, 137]. This meniscus is depicted in figure 13. The lipids residing next to the peptide, at a distance of roughly 15 Å from its centre (see figure 13), are maximally perturbed from their equilibrium position. The lipids closer to the peptide are further away from the bilayer centre because they reside with their head groups immediately above (for the upper leaflet) the hydrophilic peptide cap, with their acyl tails bent to flank the length of the hydrophobic core of the peptide.

The meniscus region draws water into it (figure 14(A)). This movement depletes the water layer far from the peptide, allowing the bilayers in these regions to come into contact and fuse (figure 14(B)). This fusion event pinches off the water sheets, trapping the water in cylindrical pores which are the hallmark of inverted phases (figure 14(C)). This mechanism is proposed to account for the experimentally observed phase transition reported by Killian [138].

6.5. Structure and dynamics of model protein insertion into a membrane

Inspired by the work of Ghadiri [44] and Hummer [49], we created a model that could both represent a transmembrane peptide with a hydrophobic core (as is common in many viral ion channels) as well as a tube-like molecule or nanotube. Two cylindrical moieties are constructed for the purpose of the simulations (see figure 15). The first consists of purely hydrophobic sites (HBT) while the second includes hydrophilic caps at both ends (HBTC). The hydrophobic length of the first tube was chosen to match the hydrophobic thickness of the lipid bilayer. The second tube was built with an additional matching to the hydrophilic head groups of the bilayer. Hydrophobic/hydrophilic matching has been shown previously to be important for transmembrane proteins [110].

From previous work we have inferred that a hydrophobic tube embedded in the membrane is not sufficient to allow the continuous passage of water molecules across the membrane. Modifications, such as the capping units, are necessary to allow the continuous flow of water, or at least the formation of a pore that does not get occluded by lipid tails. From figures 16 and 17 it is observed that the HBTC caps are anchored at the head group–water interface.

Our simulations are run in the constant temperature and pressure ensemble where the orthorhombic box size is adjusted separately in all three directions, which forces the system to have a surface tension of zero. Nevertheless, we expect local fluctuations in surface tension to be manifested in the area that a lipid head group occupies. The analysis of the change in area per head group of the individual lipids with distance from the tube is presented below both to examine the packing and as an alternative way to explore the local changes in surface tension. Use of an ensemble that permits a non-zero surface tension would not improve the study because it is the difference in local tension between the lipids in close proximity to the tube and those far from the tube that is of interest.

In figure 18 we examine the packing of the lipids around the tube through the use of Voronoi tessellations. The two-dimensional Voronoi polygons corresponding to a particular leaflet have as their centres the lipid centres of mass (COM) projected onto the bilayer plane. The polygon region of a particular lipid consists of all the points that are closer to that lipid COM than to any other lipid projected COM. The area of the tube in the bilayer plane is $316\,\text{Å}^2$ and the average area of the lipids in the first shell surrounding the tube is $64\,\text{Å}^2$. The lipids in the second shell have a larger area with a value of $69\,\text{Å}^2$ and the lipids in the remainder of the leaflet have an area per head group of $70\,\text{Å}^2$. This value of $70\,\text{Å}^2$ for the lipids far from the tube is equal to the mean area per lipid in an undisturbed (pure) lipid bilayer. From this analysis we see that the lipids tend to pack more tightly around the tube seemingly as a result of their direct interaction with HBTC.

In a more ambitious study, the HBTC is placed on top of the membrane (figure 19(A)). When the HBTC is close to the membrane, the bulk water–HBTC interaction is repulsive and anisotropic due to the presence of the membrane. This repulsion in conjunction with an attractive HBTC–membrane van der Waals interaction drives the HBTC towards the membrane. The tube then plunges into the membrane in a lateral orientation, almost perpendicular to the bilayer normal, as shown in figure 19(B). During this process some lipids become attached to the ends of the tube. Two key lipids, depicted in orange, chaperone the HBTC lower capping ring through the acyl tail region as it rotates to align perpendicular to the membrane. The tube rotation allows its hydrophobic core to become solvated by the lipid tails. This, however, implies that the hydrophilic cap in the core of the bilayer (figure 19(C)) is in an unfavourable environment along with the chaperone lipids, which remain attached due to the interaction between the lipid head groups and the tube caps. As the rotating end of the tube approaches the opposite leaflet, the chaperone lipids help the HBTC finish its rotation. Figures 19(D) and (e) show the tube in the final stages of its rotation. After the rotation is completed the chaperoning lipids join the lower leaflet and the tube remains perpendicular throughout the remainder of the simulation.

A second simulation, where a purely hydrophobic tube was placed above the membrane and allowed to insert, was seen to act with a different insertion process [139]. In this case the insertion is slower since the head group–tube interactions are unfavourable. The tube however submerges into the lipid tails and becomes solvated and quickly blocked by the tails. The long axis of the tube remains approximately parallel to the bilayer plane throughout this process.

This study suggests that it is possible for tube-like molecules, alpha helices, or nanotubes to insert spontaneously into a bilayer, even when they contain hydrophilic groups, and immersion of such species can be mediated by chaperone lipid flip-flop. Lipid transbilayer flips are

among the slowest molecular timescale events undertaken by lipids. These timescales cannot be accessed by classical atomistic molecular dynamics simulations. It is not far-fetched, however, to imagine such motions at a macroscopic level where millions of lipids are available for flipping and where other effects such as undulations and raft aggregation will have an effect on the overall dynamics of the membrane and even on HBTC-type immersion.

6.6. Antimicrobial membrane attack

Recent interest in generic classes of therapeutic agents [44, 50, 140, 40, 141–143] has lead to synthetic designs which show great potential for combating bacterial infections. Various mechanisms of action have been proposed for natural (peptidic) and synthetic antimicrobials (AM) which target the membrane [144]. Motivating the work presented here is a desire to understand the nature of poration caused by synthetic antimicrobial molecules interacting with a phospholipid membrane. The specific AM molecule considered is the amphipathic aryl amide dimer (figure 20), which is known to have potent antimicrobial activity, and which was inspired by natural and synthetic peptides [41, 50, 142, 145].

Several existing units were used to build the aryl amide antimicrobial. The positively charged section was approximated using an existing choline site, which is similar to the group we are trying to emulate. The remainder of the antimicrobial was modelled using generic hydrophobic sites and ester sites from the original model in an effort to preserve both the hydrophobic and slightly hydrophilic character of the antimicrobial bonds and the benzene ring. Special care was taken to preserve the overall size and shape of the aryl amide molecules in the coarse grain construct.

Two AM insertion mechanisms were observed in the simulations. The first consists of the spontaneous penetration of single, isolated AM molecules, which is relevant at lower concentrations when AMs do not interact. Accommodation and penetration occur with the long axis of the AM molecule remaining approximately parallel to the lipid surface. A second mechanism occurs when AM molecules interact.

Cooperative AM activity, in which one molecule possesses the capacity to interact and drag neighbouring antimicrobials into the lipid bilayer, is shown in figure 21. In the early stages of the MD simulation the AM molecules snorkel at the head group region of the outer leaflet lipid–water interface (figure 21(A)) with their hydrophilic amide groups in the water. As the simulation evolves the AM molecules dive into the membrane to reside under the head groups (figure 21(B)). At still longer times, some AM molecules cross the lipid bilayer to reside under the head groups of the inner leaflet (figure 21(C)).

All the AM molecules eventually insert into the membrane core and become oriented with their long axis parallel to the membrane surface. AM associations during the insertion process are lost via diffusion after insertion into the membrane. This accommodation and penetration mechanism of insertion differs from the traditional view of aggregation and oligomerization attributed to peptides such as magainins and melittins [140, 144]. After accommodation/penetration, the AM cationic groups reside close to the hydrated lipid phosphate and glycerol moieties while the remainder of the molecule resides in the hydrophobic core.

6.7. Buckling instabilities in Langmuir monolayers

LMs are usually studied as a function of surface coverage by either changing the number of surfactant molecules at fixed surface area A, or by changing the surface area at a fixed quantity of surfactant. Experimentally one monitors the surface pressure, $\pi = \gamma_0 - \gamma$, where γ_0 is
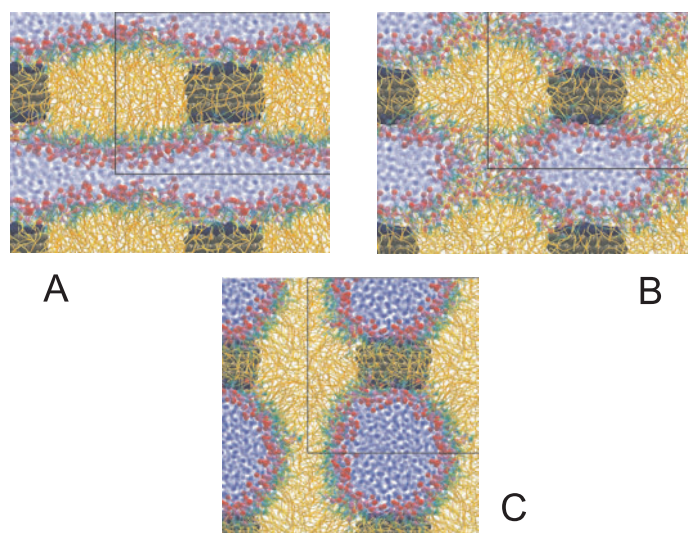
Figure 14. Membrane contact induced by the presence of a hydrophobically mismatched transmembrane peptide assembly. The simulation unit cell is shown by the black rectangle. The colouring is as follows: water blue, hydrocarbon yellow, choline red, phosphate purple, glycerol blue, ester green, and the peptide assembly in dark colours.
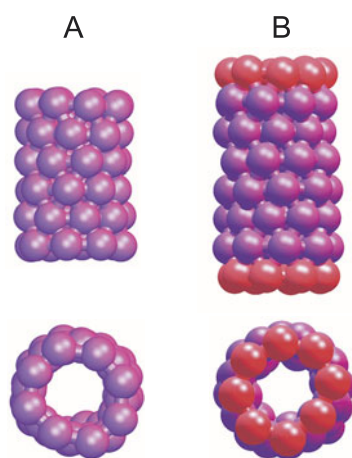

Figure 15. Hydrophobic and capped tubes. Six rings consisting of eight hydrophobic sites are stacked in a staggered manner and joined by bonds with an equilibrium length of 5 Å. Two additional rings constructed from hydrophilic sites serve to cap the second tube.

the surface tension of the pure air–water system and γ is the resultant surface tension in the presence of surfactant. Pressure–area isotherms, where π versus A is measured at constant temperature, can be mapped out and frequently show hysteresis loop behaviour as some of the surfactant is lost due to irreversible monolayer collapse [146].

At high coverage the system tends to increase its interfacial area, eventually leading to collapse of the monolayer [147]. In fact, the amplitude of the thermal fluctuations diverges as the surface tension approaches 0 (π approaches γ_0) [148]. Milner [15] showed that an ideal diblock copolymer monolayer develops a buckling instability only at zero surface
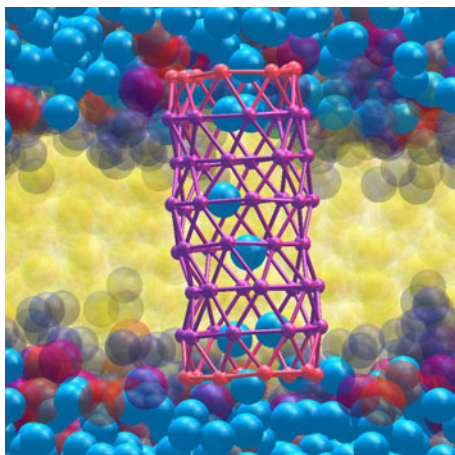
Figure 16. Water transport across a capped nanotube embedded in a lipid bilayer. A snapshot of water (blue) diffusing across the HBTC tube embedded in a CG-DMPC bilayer. The hydrophobic part of the tube is depicted in purple, and the hydrophilic caps in red. The lipid tails (yellow), phosphate unit (purple), choline unit (red), glycerol and ester groups (dark blue) are semi-transparent.
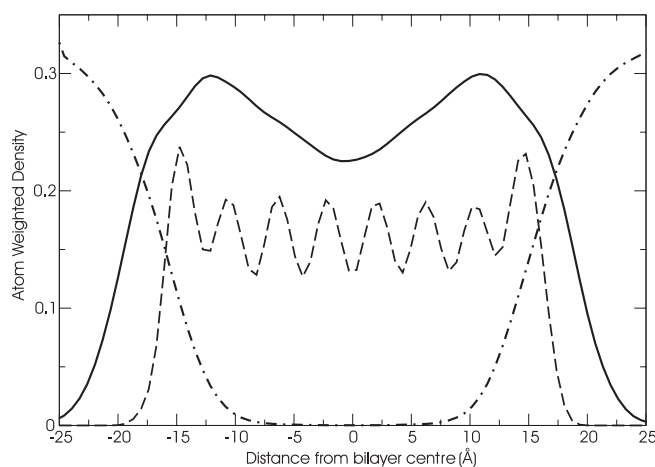

Figure 17. The density profile of a capped nanotube in a lipid bilayer. The profile shows lipid (solid curve), water (dot–dash), and HBTC (dash). The tube remains anchored at the lipid/water interface throughout the simulation.

tension. Collapse usually occurs before this limit. Collapse can occur into the solvent subphase or outwards on top of the monolayer. The outward collapse is by the formation of multilayers [149]. These multilayers can be oriented in various ways. One possibility is the formation of a trilayer by a 'rollover' mechanism in which a bilayer is formed on top of the monolayer [150]. If the bulk solution in equilibrium with the monolayer is at or above its critical micelle concentration, the monolayer may shed micelles readily into the bulk [15]. An extensive analysis of contributions to the bending free energy has been undertaken by Hu [10].

We show an example of monolayer collapse in figures 22 and 23. At first the monolayer can relieve its high surface pressure by the development of curvature (see figure 22(A)) to increase
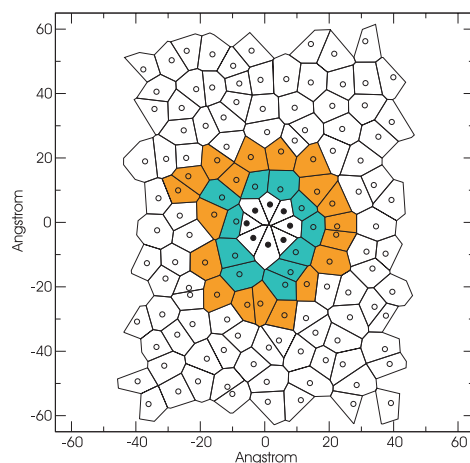
Figure 18. A depiction of the area per head group of a lipid with an embedded nanotube using Voronoi tessellations. The Voronoi diagram for the tube atoms and lipid centres of mass for one leaflet snapshot halfway through the simulation. The tube points (black filled circles) and lipid points (empty circles) are shown for each polygon. The first and second lipid shells (shaded) have different average areas per head group as discussed in the text.
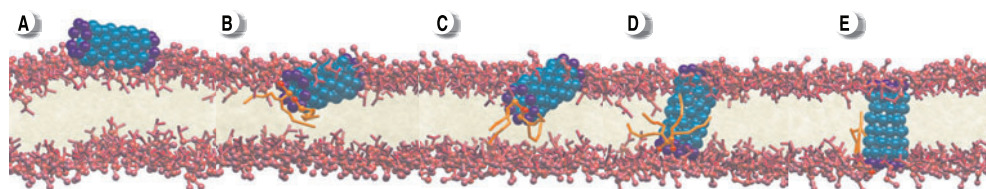

Figure 19. Spontaneous insertion of a capped hydrophobic nanotube into a phospholipid bilayer. The nanotube first adsorbs onto the membrane surface (A) and is then accommodated at the lipid–water interface (B). Lipids interacting with one of the hydrophilic capping rings chaperone the nanotube across the membrane core ((C), (D)) whereupon it assumes a stable transmembrane orientation (E).

the interfacial area. If this is not enough, lipid are shed from the monolayer. We observed [129] a loss of lipids to the exterior of the monolayer by a bridge transport mechanism, as seen in figure 22(B). This bridge minimizes the energy penalty for the head groups traversing the hydrophobic region. After enough lipids are channelled to the exterior, the monolayer stabilizes and flattens (see figure 22(C)). For the simulation of figure 22, the instantaneous surface tension versus time is shown in figure 23.

7. Future perspectives

There are three fronts along which the current CG studies can be continued. Firstly, systems can be studied whose constituent components have already been parametrized. An example of this is the study of Langmuir monolayers using existing water and phospholipid parameters as illustrated in section 6.7. Inaccuracies which come to light in such studies can point the way to improving the model, which has been parametrized from lamellar phase data. Secondly, existing parameters can be used as building blocks for new species. The antimicrobial polymer
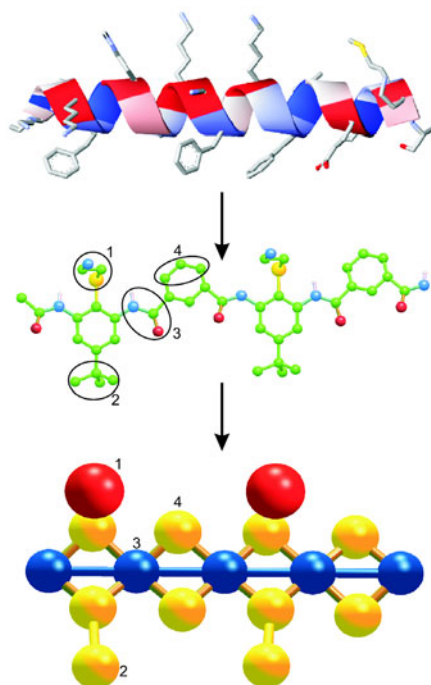
Figure 20. Molecular representation of magainin (top: α-helix, ribbon shaded by hydrophobicity; individual amino acids shown as sticks), a potent natural antimicrobial, the aryl amide molecule inspired by natural antimicrobials (middle: oxygens, dark), and its coarse grain representation (the focus of this work, bottom: hydrophobic, light). Circles in the atomistic aryl amide representation correspond to numbered units in the coarse grain representation.

discussed in section 6.6 is an example of this. Thirdly, new species can be fully parametrized from a combination of atomistic simulations and experimental observables. In addition, part of the appeal of CG simulations is that they offer an efficient way to explore ideas and hypotheses one might have about a given system. An intriguing result should be considered as a candidate for a targeted atomistic study, perhaps in combination with free energy methods using information from the CG simulation as a bias.

The appeal of the second front is that a new species can be constructed very quickly. Moreover, the construction can be artificial in the sense that some interactions can be deliberately excluded or modified in order to assess their impact on the system under study. The drawbacks to this partial parametrization are that the model loses its predictive power for specific molecular systems, and the interaction parameters may not even be amenable to a crude guess based on the existing force field. As an example of this last point, the effect of unsaturation in the lipid acyl tail cannot be mimicked on the basis of the existing saturated phospholipid parameter set.

There are numerous topics which are amenable to study with the CG method, some of which we now mention. Bilayers and monolayers involving a few lipid species and cholesterol are suitable for studying raft formation [151]. The compression/expansion cycle of the lung surfactant DPPC could be studied in the presence of the surfactant proteins (SPs) SP-A, SP-B, and SP-C, which are known to alter monolayer collapse [152]. Lipid mediated protein–protein interactions can be used to explore membrane protein crystallization [153]. The cyclic D,L-α-peptide nanotubes of Ghadiri [45] and co-workers could be studied for their self-assembly
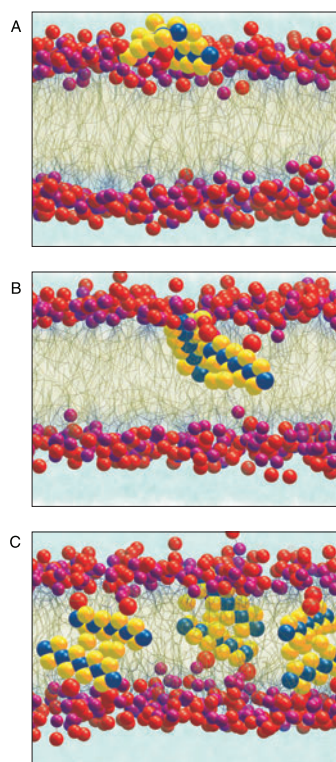
Figure 21. Insertion of CG antimicrobials into a lipid bilayer. A depiction of the two-step mechanism of insertion of AM molecules into the lipid (DMPC: head groups, balls; hydrophobic tails, sticks) bilayer ((A), (B)) and subsequent population of both monolayers at longer times (C). The accommodation stage of the mechanism involves adsorption and 'snorkeling' of the AM at the bilayer surface (A). In the penetration stage one AM rotates to become perpendicular to the bilayer plane and drags the accompanying AM into the membrane core (B). At longer times AMs can flip-flop and populate both leaflets (C).
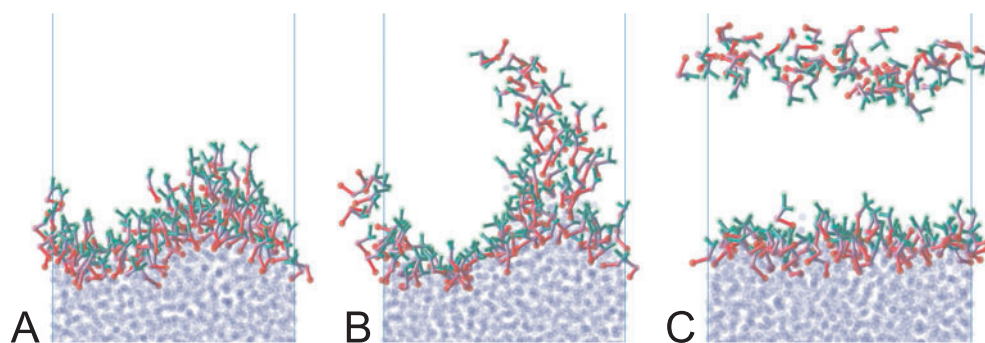

Figure 22. Monolayer instability and collapse shown at one interface of a system with 120 lipids per interface. The initially flat interface (not shown) develops some curvature (panel (A)) and then opens a bridge to the exterior of the leaflet (panel (B)). This bridge transports enough material to eventually bring the system back into equilibrium with a flat monolayer interface (panel (C)). See figure 23 for the time and the surface tension of these snapshots. Acyl tails are not shown.
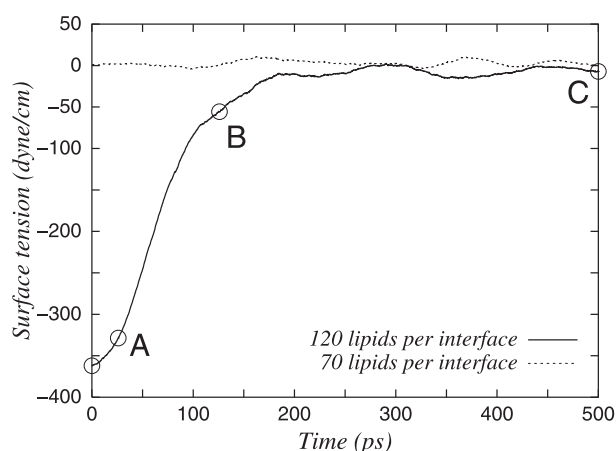
Figure 23. Instantaneous surface tension (dyn cm^{-1}) versus raw simulation time (ps) for the unstable system with 120 lipids per interface shown in figure 22. The data are smoothed with a 100 ps wide symmetrical second-order Savitzky–Golay filter [64]. Shown for comparison is the corresponding curve for the case with 70 lipids per interface, which has a surface tension of roughly zero (corresponding to a surface pressure of roughly 72 dyn cm^{-1}). The four points marked on the plot are as follows from left to right. The first point corresponds to the initially flat monolayer with 120 lipids per interface. The second point corresponds to figure 22(A) when the interface has developed curvature. The third point corresponds to figure 22(B) when the monolayer is expelling lipids. The fourth point corresponds to figure 22(C) when the monolayer has come to equilibrium.

and membrane disruption [44] properties. Monolayer structure at solid/water interfaces [154] displays novel geometry such as a hemicylindrical micelles which is being elucidated with atomic force microscopy [155]. Entropic and enthalpic interactions between amphiphile surfaces [8, 7] such as micelles, lipid bilayers, microemulsion droplets, and combinations thereof can be computed as potentials of mean force. Protein alignment can be studied as a function of surface pressure in Langmuir monolayers [156]. Self-assembled vesicles from non-lipid species such as surfactant-like peptides [157] or block copolymers offer alternatives for many applications including targeted drug delivery: typically a hydrolytically susceptible polyester such as polylactic acid is introduced into the vesicle [158]. In conclusion, there are clearly many possible future applications of CG models.

Acknowledgments

References

[1] Li P-C and Makarov D E 2003 *J. Chem. Phys.* **119** 9260
[2] Rafii-Tabar H and Chirazi A 2002 *Phys. Rep.* **365** 145
[3] N'Dri N A, Shyy W and Tran-Son-Tay R 2003 *Biophys. J.* **85** 2273
[4] Goddard W A III, Cagin T, Blanco M, Vaidehi N, Dasgupta S, Floriano W, Belmares M, Kua J, Zamanakos G, Kashihara S, Iotov M and Gao G 2001 *Comput. Theor. Polym. Sci.* **11** 329

[5] Muralidharan K, Deymier P A and Simmons J H 2003 *Modelling Simul. Mater. Sci. Eng.* **11** 487

[6] Svoboda K and Block S M 1994 *Annu. Rev. Biophys. Biomol. Struct.* **23** 247

[7] Safran S A 1994 *Statistical Thermodynamics of Surfaces, Interfaces, and Membranes* (New York: Addison-Wesley)

[8] Israelachvili J and Wennerström H 1992 *J. Phys. Chem.* **96** 520

[9] Marsh D 1996 *Biochim. Biophys. Acta* **1286** 183

[10] Hu J-G and Granek R 1996 *J. Physique* II **6** 999

[11] Walz J Y and Ruckenstein E 1999 *J. Phys. Chem.* B **103** 7461

[12] Sens P and Safran S A 2000 *Eur. Phys. J.* E **1** 237

[13] Fattal D R and Ben-Shaul A 1993 *Biophys. J.* **65** 1795

[14] May S and Ben-Shaul A 1999 *Biophys. J.* **76** 751

[15] Milner S T, Joanny J-F and Pincus P 1989 *Europhys. Lett.* **9** 495

[16] Duque D, Li X, Katsov K and Schick M 2002 *J. Chem. Phys.* **116** 10478

[17] Nielsen C, Goulian M and Andersen O S 1998 *Biophys. J.* **74** 1966

[18] Harroun T A, Heller W T, Weiss T M, Yang L and Huang H W 1999 *Biophys. J.* **76** 3176

[19] Tries V, Paul W, Baschnagel J and Binder K 1997 *J. Chem. Phys.* **106** 738

[20] Fukunaga H, Takimoto J and Doi M 2002 *J. Chem. Phys.* **116** 8183

[21] Müller-Plathe F 2002 *Chem. Phys. Chem.* **3** 754

[22] Akkermans R L C and Briels W J 2001 *J. Chem. Phys.* **114** 1020

[23] Nielsen S O, Lopez C F, Srinivas G and Klein M L 2003 *J. Chem. Phys.* **119** 7043

[24] Stevens M J, Hoh J H and Woolf T B 2003 *Phys. Rev. Lett.* **91** 188102

[25] Marrink S J and Mark A E 2003 *J. Am. Chem. Soc.* **125** 11144

[26] Shelley J C, Shelley M Y, Reeder R C, Bandyopadhyay S and Klein M L 2001 *J. Phys. Chem.* B **105** 4464

[27] Sprong H, van der Sluijs P and van Meer G 2001 *Nat. Rev. Mol. Cell Biol.* **2** 504

[28] Li X and Schick M 2000 *J. Chem. Phys.* **112** 10599

[29] Jahn R and Grubmüller H 2002 *Curr. Opin. Cell Biol.* **14** 488

[30] Dumas F, Lebrun M C and Tocanne J-F 1999 *FEBS Lett.* **458** 271

[31] Brown M F, Thurmond R L, Dodd S W, Otten D and Beyer K 2001 *Phys. Rev.* E **64** 010901

[32] McIntosh T J 2000 *Curr. Opin. Struct. Biol.* **10** 481

[33] Dufrêne Y F, Boland T, Schneider J W, Barger W R and Lee G U 1998 *Faraday Discuss.* **111** 79

[34] Cornelissen J J L M, Fischer M, Sommerdijk N A J M and Nolte R J M 1998 *Science* **280** 1427

[35] Hillmyer M A and Bates F S 1996 *Macromolecules* **29** 6994

[36] Zhang L and Eisenberg A 1995 *Science* **268** 727

[37] Discher B M, Won Y-Y, Ege D S, Lee J C-M, Bates F S, Discher D E and Hammer D A 1999 *Science* **284** 1143

[38] Pakula T, Karatasos T, Anastasiadis S H and Fytes G 1997 *Macromolecules* **30** 8463

[39] Schultz A J, Hall C K and Genzer J 2002 *J. Chem. Phys.* **117** 10329

[40] Bayley H 1999 *Curr. Opin. Biotechnol.* **10** 94

[41] Tew G N, Liu D, Chen B, Doerksen R J, Kaplan J, Carroll P J, Klein M L and DeGrado W F 2002 *Proc. Natl Acad. Sci. USA* **99** 5110

[42] Zhong Q F, Jiang Q, Moore P B, Newns D M and Klein M L 1998 *Biophys. J.* **74** 3

[43] Lee S B, Mitchell D T, Trofin L, Nevanen T K, Soderlund H and Martin C R 2002 *Science* **296** 2198

[44] Fernandez-Lopez S, Kim H-S, Choi E C, Delgado M, Granja J R, Khasanov A, Kraehenbuehl K, Long G, Weinberger D A, Wilcoxen K M and Ghadiri M R 2001 *Nature* **412** 452

[45] Hartgerink J D, Clark T D and Ghadiri M R 1998 *Chem. Eur. J.* **4** 1367

[46] Kim H S, Hartgerink J D and Ghadiri M R 1998 *J. Am. Chem. Soc.* **118** 43

[47] Asthagiri D and Bashford D 2002 *Biophys. J.* **82** 1176

[48] Discher B M, Bermudez H, Hammer D A, Discher D A, Won Y Y and Bates F S 2002 *J. Phys. Chem.* B **106** 2848

[49] Hummer G, Rasaiah J C and Noworyta J P 2001 *Nature* **414** 188

[50] Zasloff M 2002 *Nature* **415** 389

[51] Hoffmann J A, Kafatos F C, Janeway C A Jr and Ezekowitz R A B 1999 *Science* **284** 1313

[52] Andreu D and Rivas L 1998 *Biopolymers* **47** 415

[53] La Rocca P, Shai Y and Sansom M S P 1999 *Biophys. Chem.* **76** 145

[54] Glotzer S C and Paul W 2002 *Annu. Rev. Mater. Res.* **32** 401

[55] Carmesin I and Kremer K 1988 *Macromolecules* **21** 2819

[56] Deutsch H P and Binder K 1991 *J. Chem. Phys.* **94** 2294

[57] Chen C-M and Higgs P G 1998 *J. Chem. Phys.* **108** 4305

[58] Chen C-M and Chen C-C 2003 *Biophys. J.* **84** 1902
[59] Wu Z-B, Diestler D J, Feng R and Zeng X C 2003 *J. Chem. Phys.* **119** 8013
[60] Mobley D L, Cox D L, Singh R R P, Kulkarni R V and Slepoy A 2003 *Biophys. J.* **85** 2213
[61] van Heukelum A and Barkema G T 2003 *J. Chem. Phys.* **119** 8197
[62] Anderson H 1983 *J. Comput. Phys.* **52** 24
[63] McCoy J D and Curro J G 1998 *Macromolecules* **31** 9362
[64] Press W H, Teukolsky S A, Vetterling W T and Flannery B P 1992 *Numerical Recipes in Fortran 77: the Art of Scientific Computing* 2nd edn (New York: Cambridge University Press)
[65] Izaguirre J A, Catarello D P, Wozniak J M and Skeel R D 2001 *J. Chem. Phys.* **114** 2090
[66] Mori H 1965 *Prog. Theor. Phys.* **33** 423
[67] Chorin A J, Hald O H and Kupferman R 2000 *Proc. Natl Acad. Sci. USA* **97** 2968
[68] Zou G and Skeel R D 2003 *Biophys. J.* **85** 2147
[69] ten Wolde P R and Chandler D 2002 *Proc. Natl Acad. Sci. USA* **99** 6539
[70] Malevanets A and Kapral R 2000 *J. Chem. Phys.* **112** 7260
[71] David L, Luo R and Gilson M K 2000 *J. Comput. Chem.* **21** 295
[72] Im W, Feig M and Brooks C L III 2003 *Biophys. J.* **85** 2900
[73] Flekkøy E G and Coveney P V 1999 *Phys. Rev. Lett.* **83** 1775
[74] Kranenburg M, Venturoli M and Smit B 2003 *J. Phys. Chem.* B **107** 11491
[75] Groot R D and Rabone K L 2001 *Biophys. J.* **81** 725
[76] Flory P J 1953 *Principles of Polymer Chemistry* (Ithaca, NY: Cornell University Press)
[77] Liwo A, Ołdziej S, Pincus M R, Wawak R J, Rackovsky S and Scheraga H A 1997 *J. Comput. Chem.* **18** 849
[78] Kolinski A and Skolnick J 1992 *J. Chem. Phys.* **97** 9412
[79] Cagin T, Wang G, Martin R, Zamanakos G, Vaidehi N, Mainz D T and Goddard W A III 2001 *Comput. Theor. Polym. Sci.* **11** 345
[80] Whitehead L, Edge C M and Essex J W 2001 *J. Comput. Chem.* **22** 1622
[81] Padding J T and Briels W J 2002 *J. Chem. Phys.* **117** 925
[82] Groot R D 2003 *J. Chem. Phys.* **118** 11265
[83] Tabacchi G, Mundy C J, Hutter J and Parrinello M 2002 *J. Chem. Phys.* **117** 1416
[84] Lyubartsev A P and Laaksonen A 1995 *Phys. Rev.* E **52** 3730
[85] McGreevy R L and Pusztai L 1988 *Mol. Simul.* **1** 359
[86] Kalé L, Skeel R, Bhandarkar M, Brunner R, Gursoy A, Krawetz N, Phillips J, Shinozaki A, Varadarajan K and Schulten K 1999 *J. Comput. Phys.* **151** 283
[87] Karaborni S, Esselink K, Hilbers P A J, Smit B, Karthäuser J, van Os N M and Zana R 1994 *Science* **266** 254
[88] Larson R G, Scriven L E and Davis H T 1985 *J. Chem. Phys.* **83** 2411
[89] Larson R G 1989 *J. Chem. Phys.* **91** 2479
[90] Larson R G 1994 *Chem. Eng. Sci.* **49** 2833
[91] Paul W and Pistoor N 1994 *Macromolecules* **27** 1249
[92] Scott H L 2002 *Curr. Opin. Struct. Biol.* **12** 495
[93] Bermudez H, Brannan A K, Hammer D A, Bates F S and Discher D E 2002 *Macromolecules* **35** 8203
[94] Li Z X, Dong C C, Wang J B and Thomas R K 2002 *Langmuir* **18** 6614
[95] Demond A H and Lindner A S 1993 *Environ. Sci. Technol.* **27** 2318
[96] Bandyopadhyay S, Shelley J C and Klein M L 2001 *J. Phys. Chem.* B **105** 5979
[97] Faller R, Schmitz H, Biermann O and Müller-Plathe F 1999 *J. Comput. Chem.* **20** 1009
[98] http://software.sandia.gov/appspack/
[99] Katsoulakis M A and Vlachos D G 2003 *J. Chem. Phys.* **119** 9412
[100] Louis A A 2002 *J. Phys.: Condens. Matter* **14** 9187
[101] Tóth G and Baranyai A 2001 *J. Chem. Phys.* **114** 2027
[102] Harper P E, Mannock D A, Lewis R N A H, McElhaney R N and Gruner S M 2001 *Biophys. J.* **81** 2693
[103] Rudek M M, Fisk J A, Chakarov V M and Katz J L 1996 *J. Chem. Phys.* **105** 4707
[104] Shelley J C, Shelley M Y, Reeder R C, Bandyopadhyay S, Moore P B and Klein M L 2001 *J. Phys. Chem.* B **105** 9785
[105] Whittington S G 2000 *Fields Inst. Commun.* **26** 131
[106] Opps S B and Schofield J 2001 *Phys. Rev.* E **63** 056701
[107] Lopez C F, Moore P B, Shelley J C, Shelley M Y and Klein M L 2002 *Comput. Phys. Commun.* **147** 1
[108] Lopez C F, Nielsen S O, Moore P B, Shelley J C and Klein M L 2002 *J. Phys.: Condens. Matter* **14** 9431
[109] von Meerwall E, Beckman S, Jang J and Mattice W L 1998 *J. Chem. Phys.* **108** 4299
[110] Moore P B, Lopez C F and Klein M L 2002 *Biophys. J.* **81** 2484
[111] Linse P and Lobaskin V 2000 *J. Chem. Phys.* **112** 3917

[112] Basu J K and Sanyal M K 2002 *Phys. Rep.* **363** 1
[113] Chiu S W, Vasudevan S, Jakobsson E, Mashl R J and Scott H L 2003 *Biophys. J.* **85** 3624
[114] Goetz R, Gompper G and Lipowsky R 1999 *Phys. Rev. Lett.* **82** 221
[115] Marrink S J and Mark A E 2001 *J. Phys. Chem.* B **105** 6122
[116] Lindahl E and Edholm O 2000 *Biophys. J.* **79** 426
[117] Hirn R, Bayerl T M, Rädler J O and Sackmann E 1998 *Faraday Discuss.* **111** 17
[118] den Otter W K and Briels W J 2003 *J. Chem. Phys.* **118** 4712
[119] Goetz R and Lipowsky R 1998 *J. Chem. Phys.* **108** 7397
[120] Drouffe J-M, Maggs A C and Leibler S 1991 *Science* **254** 1353
[121] Noguchi H and Takasu M 2001 *Phys. Rev.* E **64** 041913
[122] Smit B, Esselink K, Hilbers P A J, van Os N M, Rupert L A M and Szleifer I 1993 *Langmuir* **9** 9
[123] Yamamoto S, Maruyama Y and Hyodo S 2002 *J. Chem. Phys.* **116** 5842
[124] von Gottberg F K, Smith K A and Hatton T A 1997 *J. Chem. Phys.* **106** 9850
[125] von Gottberg F K, Smith K A and Hatton T A 1998 *J. Chem. Phys.* **108** 2232
[126] Marrink S J, Tieleman D P and Mark A E 2000 *J. Phys. Chem.* B **104** 12165
[127] Marrink S J, Lindahl E, Edholm O and Mark A E 2001 *J. Am. Chem. Soc.* **123** 8638
[128] Bogusz S, Venable R M and Pastor R W 2001 *J. Phys. Chem.* B **105** 8312
[129] Nielsen S O, Lopez C F, Moore P B, Shelley J C and Klein M L 2003 *J. Phys. Chem.* B **107** 13911
[130] Israelachvili J 1991 *Intermolecular and Surface Forces* (New York: Academic)
[131] Wang Q, Nealey P F and de Pablo J J 2001 *Macromolecules* **34** 3458
[132] de Planque M R R, Goormaghtigh E, Greathouse D V, Koeppe R E II, Kruijtzer J A W, Liskamp R M J,
      de Kruijff B and Killian J A 2001 *Biochemistry* **40** 5000
[133] Harroun T A, Heller W T, Weiss T M, Yang L and Huang H W 1999 *Biophys. J.* **76** 937
[134] Gill T, Ipsen J H, Mouritsen O G, Sabra M C, Sperotto M M and Zuckermann M J 1998 *Biochim. Biophys.*
      Acta **1376** 245
[135] Wahab M, Mögel H-J and Schiller P 2001 *Mol. Phys.* **99** 2045
[136] de Planque M R R, Greathouse D V, Koeppe R E II, Schäfer H, Marsh D and Killian J A 1998 *Biochemistry*
      37 9333
[137] Petrache H I, Zuckerman D M, Sachs J N, Killian J A, Koeppe R E II and Woolf T B 2002 *Langmuir* **18** 1340
[138] Killian J A, Salemink I, de Planque M R R, Lindblom G, Koeppe R E II and Greathouse D V 1996 *Biochemistry*
      35 1037
[139] Lopez C F, Nielsen S O, Moore P B and Klein M L 2004 *Proc. Natl Acad. Sci. USA* **101** 4431
[140] Yang L, Harroun Y A, Weiss T M, Ding L and Huang H W 2001 *Biophys. J.* **81** 1475
[141] Lear J D, Gratkowski H L and DeGrado W F 2001 *Biochem. Soc.* **29** 559
[142] Raguse T L, Porter E A, Weisblum B and Gellman S H 2002 *J. Am. Chem. Soc.* **124** 12774
[143] Patch J A and Barron A E 2003 *J. Am. Chem. Soc.* **125** 12092
[144] Shai Y 2002 *Biopolymers* **66** 236
[145] Porter E A, Wang X F, Lee H S, Weisblum B and Gellman S H 2000 *Biophys. J.* **84** 565
[146] Lipp M M, Lee K Y C, Takamoto D Y, Zasadzinski J A and Waring A J 1998 *Phys. Rev. Lett.* **81** 1650
[147] Ridsdale R A, Palaniyar N, Possmayer F and Harauz G 2001 *J. Membr. Biol.* **180** 21
[148] Schief W R, Touryan L, Hall S B and Vogel V 2000 *J. Phys. Chem.* B **104** 7388
[149] Ybert C, Lu W, Möller G and Knobler C M 2002 *J. Phys. Chem.* B **106** 2004
[150] Ybert C, Lu W, Möller G and Knobler C M 2002 *J. Phys.: Condens. Matter* **14** 4753
[151] Pralle A, Keller P, Florin E-L, Simons K and Hörber J K H 2000 *J. Cell Biol.* **148** 997
[152] Veldhuizen E J A and Haagsman H P 2000 *Biochim. Biophys. Acta* **1467** 255
[153] Caffrey M 2000 *Curr. Opin. Struct. Biol.* **10** 486
[154] Bandyopadhyay S, Shelley J C, Tarek M, Moore P B and Klein M L 1998 *J. Phys. Chem.* B **102** 6318
[155] Grant L M, Tiberg F and Ducker W A 1998 *J. Phys. Chem.* B **102** 4288
[156] Tronin A, Strzalka J, Chen X, Dutton P L, Ocko B M and Blasie J K 2001 *Langmuir* **17** 3061
[157] Vauthey S, Santoso S, Gong H, Watson N and Zhang S 2002 *Proc. Natl Acad. Sci. USA* **99** 5355
[158] Shah S S, Zhu K J and Pitt C G 1994 *J. Biomater. Sci. Polym. Edn* **5** 421